

Interdecadal change in the lagged relationship between the Pacific–South American pattern and ENSO

Ruiqiang Ding^{1,2} · Jianping Li^{3,4} · Yu-heng Tseng⁵ · Kyung-Ja Ha^{6,7} · Sen Zhao¹ ·
June-Yi Lee⁷

Received: 10 October 2015 / Accepted: 18 January 2016 / Published online: 28 January 2016
© Springer-Verlag Berlin Heidelberg 2016

Abstract A significant interdecadal change in the lagged relationship between the austral summer Pacific–South American (PSA) pattern and the El Niño–Southern Oscillation (ENSO) in the following austral summer (the PSA serving as a precursor signature to ENSO events) has been detected by analysis of a 91-year historical record. Strong correlations between the PSA and ENSO occurred during the periods 1956–1975 and 1990–2004 [referred to as the high correlation (HC) periods], but the correlations were weak for the periods 1928–1956 and 1975–1990 [referred to as the low correlation (LC) periods]. Both the processes of surface air–sea coupling in the extratropical/tropical Pacific, and subsurface ocean temperature evolution along the equator associated with the PSA, were found to be stronger during the HC periods than during the LC periods,

thereby resulting in a stronger influence of the PSA on the subsequent ENSO during the HC periods. Changes in the PSA–ENSO relationship can be attributed mainly to interdecadal changes in the intensity of the austral summer PSA. The latter was found to have contributions from both the modulation of the Pacific decadal oscillation and long-term variations in the Southern Annular Mode.

Keywords ENSO · The Pacific–South American (PSA) pattern · The Pacific decadal oscillation (PDO) · The Southern Annular Mode (SAM)

1 Introduction

The El Niño–Southern Oscillation (ENSO) phenomenon, which originates in the tropical Pacific, is the strongest of the naturally occurring interannual climate signals. ENSO has a widespread effect, not only in the tropics, but also in extratropical regions. By shifting tropical convection and the associated anomalous heating, ENSO can excite Rossby wave trains that can then propagate into higher latitudes (Horel and Wallace 1981; Hoskins and Karoly 1981). These Rossby wave trains are known as the Pacific–North America (PNA) teleconnection pattern in the Northern Hemisphere (NH) (Wallace and Gutzler 1981), and the Pacific–South American (PSA) teleconnection pattern in the Southern Hemisphere (SH) (Mo and Ghil 1987). The PNA has been shown to influence the Aleutian Low, the Asian jet, and the Pacific storm track, which subsequently affect weather and climate conditions over the North Pacific and North America (Straus and Shukla 2002; Compo and Sardeshmukh 2004). The PSA has been found to be associated with variations in the westerlies over the South Pacific, which may then affect precipitation over New Zealand, air

✉ Jianping Li
ljp@bnu.edu.cn

¹ State Key Laboratory of Numerical Modeling for Atmospheric Sciences and Geophysical Fluid Dynamics (LASG), Institute of Atmospheric Physics, Chinese Academy of Sciences, Beijing 100029, China

² Plateau Atmosphere and Environment Key Laboratory of Sichuan Province, Chengdu University of Information Technology, Chengdu 610225, China

³ College of Global Change and Earth System Sciences (GCESS), Beijing Normal University, Beijing 100875, China

⁴ Joint Center for Global Change Studies, Beijing 100875, China

⁵ Climate and Global Dynamics Division, NCAR, Boulder, CO, USA

⁶ Department of Atmospheric Sciences, Pusan National University, Busan 609-735, Korea

⁷ Research Center for Climate Sciences, Pusan National University, Busan 609-735, Korea

temperature and sea ice over the Antarctic Peninsula, and the frequency of blocking events across the high-latitude South Pacific (Renwick and Revell 1999; Kwok and Comiso 2002; Renwick 2002; Yuan 2004). In this way, both the PNA and PSA play an important role in extending the influence of ENSO from the tropics to the mid–high latitudes of both hemispheres.

In contrast to the above studies, which documented the significant influence of ENSO on mid–high latitude atmospheric variability, other studies have suggested that this mid–high latitude atmospheric variability could instead have an impact on ENSO itself (Vimont et al. 2001, 2003a, b; Anderson 2003; Alexander et al. 2010; Yu and Kim 2011). Most of these studies identified the North Pacific Oscillation (NPO) (Walker and Bliss 1932; Rogers 1981), the second leading internal atmospheric mode over the North Pacific in winter, as an important source of extratropical forcing for interannual ENSO variability. The underlying mechanisms responsible for the connection between the NPO and ENSO have been widely investigated in the literature (e.g., Vimont et al. 2003a, b; Anderson 2004, 2013; Chiang and Vimont 2004; Chang et al. 2007; Ding et al. 2015a). Two mechanisms have been proposed to explain the influence of the NPO on ENSO. First, the wintertime NPO can force a tripole-like sea surface temperature anomaly (SSTA) pattern in the North Pacific, and this SST footprint persists into late spring and summer through the wind–evaporation–SST (WES) feedback (Xie and Philander 1994), when it can subsequently force the overlying atmosphere, resulting in zonal wind anomalies over the equatorial Pacific that favor the initiation of an ENSO event; i.e., the seasonal footprinting mechanism (SFM) (Vimont et al. 2003a, b). Secondly, the NPO-induced variations in the North Pacific trade winds may produce concurrent subsurface temperature and heat content anomalies in the central and eastern tropical Pacific that are conducive to initiating an ENSO event; i.e., the trade wind charging (TWC) mechanism (Anderson 2004; Anderson et al. 2013). In addition, previous studies have shown that the Pacific meridional mode (PMM) (Chiang and Vimont 2004; Chang et al. 2007) characterized by an anomalous north–south SSTA gradient in the tropical eastern Pacific coupled with anomalous off-equatorial trade wind variability, is generally consistent with the SFM, and may work as a conduit that connects the extratropical atmospheric variability to ENSO.

However, in the South Pacific, few studies have investigated the influence of the mid–high latitude atmospheric variability on ENSO. An early study by Trenberth and Shea (1987) suggested that changes in sea level pressure (SLP) over the South Pacific lead the Southern Oscillation (SO) by 1–2 seasons. Jin and Kirtman (2009) reported that the ENSO-forced atmospheric response in the extratropical South Pacific (i.e., the PSA pattern) leads the peak phase

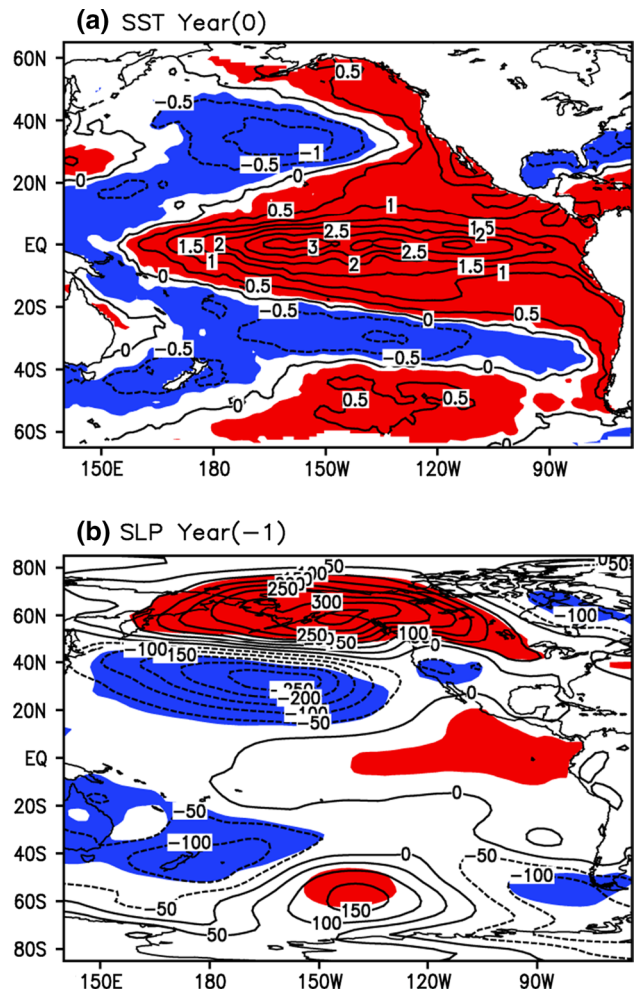


Fig. 1 Composite difference of the SST and SLP anomalies for strong ENSO cases (El Niño – La Niña): **a** Simultaneous SST averaged over November–March (NDJFM), contour interval 0.5 °C; **b** SLP (NDJFM-averaged) 1 year earlier than the SST map, contour interval 0.5 hPa. Positive (red) and negative (blue) SST and SLP anomalies, significant at the 90 % level, are shaded. Strong El Niño and La Niña cases are defined by the NDJFM-averaged ENSO index (plotted in Fig. 2c) greater than one positive standard deviation (SD) and less than one negative SD, respectively

of ENSO by one season. A further analysis of the lead–lag relationships between extratropical atmospheric variability over the South and North Pacific and ENSO was performed by Ding et al. (2015a, b), who found that in addition to the preceding NPO signal over the North Pacific, the PSA-like pattern over the South Pacific tends to precede the peak phase of ENSO by about 1 year (see also Fig. 1). They demonstrated that the process involving the surface air–sea coupling associated with the PSA in the tropical/extratropical Pacific, which resembles the SFM (Vimont et al. 2003a, b), plays an important role in triggering the onset of ENSO. That is, during the austral summer, the PSA-like atmospheric variability in the extratropical South Pacific imparts

a quadrupole SSTA pattern onto the ocean, and this SST footprint then persists into the austral late autumn and winter and extends into the deep tropics, subsequently forcing the zonal wind anomalies along the equator that ultimately lead to an ENSO event during the following austral summer via a positive ocean–atmosphere feedback in the tropics. In addition, Ding et al. (2015b) further suggested that evolution of subsurface ocean temperature anomalies along the equator associated with the PSA, which resembles the TWC (Anderson 2004; Anderson et al. 2013), also plays an important role in developing ENSO. Hereafter, we denote the ENSO-developing year as year 0 and the preceding and following years as years -1 and $+1$, respectively.

ENSO and its teleconnections (including both the PNA and PSA patterns) vary over decadal and longer timescales in both observations and coupled models (e.g., Wang and Ropelewski 1995; Wang and Wang 1996; Gershunov and Barnett 1998; McCabe and Dettinger 1999; Mann et al. 2000; Hunt and Elliott 2003; Power et al. 2006; Wu et al. 2012). Given that the austral summer PSA could again exert a forcing effect on ENSO in the following austral summer, the question naturally arises as to whether there exists a remarkable decadal change in their relationship. Ding et al. (2015b) indicated that this is indeed the case, and the correlation between the austral summer PSA and ENSO in the following austral summer was relatively weak in the 1980s, but increased after the early 1990s. However, the mechanisms that caused this change in the PSA–ENSO relationship remain unknown. The purpose of this study is to reexamine the decadal change in the relationship between the austral summer PSA and ENSO in the following austral summer, using longer datasets (back to 1921) than were used by Ding et al. (2015b), and to explore the possible causes of such changes in the PSA–ENSO relationship.

The remainder of this manuscript is organized as follows. Data and methodology are described in Sect. 2. In Sect. 3, we document the interdecadal change in the relationship between the austral summer PSA and ENSO in the following austral summer. Section 4 compares the PSA-related atmospheric and oceanic anomalies between the relatively stronger and weaker phases of the PSA–ENSO relationship. Section 5 addresses the possible causes of the change in the PSA–ENSO relationship. Finally, Sect. 6 summarizes the major findings of this study.

2 Data and methods

2.1 Data

We used the monthly mean SST field from the Hadley Center Sea Ice and SST dataset (HadISST) (Rayner

et al. 2006) and the National Oceanic and Atmospheric Administration (NOAA) Extended Reconstructed SST version 3b (ERSSTv3b) (Smith et al. 2008). The HadISST dataset has a horizontal resolution of $1^\circ \times 1^\circ$ and is available from 1870 to the present. The ERSSTv3b dataset has a horizontal resolution of $2^\circ \times 2^\circ$ and runs from 1854 to the present. We used the monthly mean subsurface ocean temperature from the Simple Ocean Data Assimilation (SODA) reanalysis for the period 1871–2008 (Giese and Ray 2011). The SODA dataset has 23 vertical levels unevenly distributed from 5 to 1139 m, and covers the global oceans from 30.75°S to 30.75°N with a horizontal resolution of $0.5^\circ \times 0.5^\circ$. The monthly mean atmospheric fields used in this study were obtained from the NOAA 20th Century Reanalysis version 2 (20CRv2) covering the period 1871–2010 with a horizontal resolution of $2^\circ \times 2^\circ$ (Compo et al. 2011). We also used the Hadley Centre's monthly mean SLP (HadSLP2r) on a $5^\circ \times 5^\circ$ spatial grid for the period 1850–2012 (Allan and Ansell 2006) and the National Centers for Environmental Prediction (NCEP1) reanalysis data on a $2.5^\circ \times 2.5^\circ$ grid for the period 1948–2012 (Kalnay et al. 1996) to verify results from 20CRv2. The Southern Oscillation Index (SOI) was calculated using the monthly SLP differences between Tahiti and Darwin, Australia, obtained from the Climate Prediction Center (CPC, see online at <http://www.cpc.noaa.gov>).

For all variables, the monthly anomalies were calculated by subtracting the climatological mean annual cycle for the 1981–2010 base period. The focus of this study, the interdecadal change in the PSA–ENSO correlation, is not sensitive to this choice of base period. We analyzed the interdecadal change in the relationship between the austral summer PSA and ENSO in the following austral summer based on the period 1921–2011, and we will show later (Figs. 3a, 4) that this period encompasses dramatic changes in their relationship.

2.2 Effective number of degrees of freedom

For the correlation between the monthly data of two variables X and Y , the effective sample size N^* was estimated using the modified Chelton method (Pypar and Peterman 1998; Li et al. 2012, 2013). N^* can be obtained from the theoretical approximation:

$$N^* \approx \frac{N}{1 + 2 \sum_{i=1}^N \frac{N-i}{N} R_X(i) R_Y(i)}, \quad (1)$$

where N is the number of available time steps and $R_X(i)$ and $R_Y(i)$ are the autocorrelations of the two sampled time series $X(i)$ and $Y(i)$ ($i = 1, \dots, N$), respectively.

3 Interdecadal change in the PSA–ENSO relationship

The canonical PSA pattern is usually obtained from the empirical orthogonal function (EOF) analysis of the SH 500 hPa seasonal mean geopotential height (GHT) anomalies (Mo 2000). The first EOF mode (EOF1) is the Southern Annular Mode [SAM; also known as the Antarctic Oscillation (AAO)] (Gong and Wang 1999; Thompson and Wallace 2000; Wu et al. 2009, 2015) that exhibits a zonally symmetric but out-of-phase height anomalies at high- and mid-latitudes, and the second and third EOF modes (EOF2 and EOF3) correspond to the PSA patterns (PSA1 and PSA2, respectively; with their phases nearly in quadrature with each other) that depict a zonal wavenumber 3 structure and a notable wave train from the tropical Pacific to Argentina with large amplitudes in the PSA sector. The projection of height anomalies onto the PSA patterns then defines the time-varying PSA indices.

Here, to show the lead–lag relationship between the SH extratropical atmospheric variability and ENSO, we used a maximum covariance analysis [MCA; also known as singular value decomposition (SVD)] (Bretherton et al. 1992) to obtain the pattern of atmospheric variability preceding ENSO and its corresponding index. MCA was performed on the cross-covariance matrix between the austral summer(−1) South Pacific (140°E–68°W, 80°–20°S) SLP anomalies from 20CRv2, and the following austral summer(0) tropical Pacific (125°E–75°W, 20°S–20°N) SST anomalies (SSTAs) from HadISST. Here, the terms austral summer(−1) and summer(0) refer to the consecutive seasons over which extratropical SLP [November–March (NDJFM)] and tropical SST [October–February (ONDJF)] are averaged. Jin and Kirtman (2009) also performed a similar MCA analysis but using the SH 500 hPa seasonal mean GHT anomalies as the leading field, which resulted in the identification of the precursor PSA pattern for ENSO events.

The leading MCA mode explains 64 % of the total squared covariance. The correlation coefficient between the corresponding expansion coefficients is 0.41 for the period 1921–2011 (Fig. 2c), which is significant at the 99.9 % level. Figure 2a, b show the leading pair of heterogeneous patterns, which are generated by correlating the respective heterogeneous SLP and SST fields with the MCA leading normalized expansion coefficients. The austral summer(−1) South Pacific SLP pattern exhibits a PSA-type wave train from the mid-latitude southwestern Pacific to the southeastern Pacific off the southwest coast of Argentina. We note that this MCA SLP pattern bears a resemblance to the PSA1 pattern shown in Fig. 1 of Mo (2000) for all seasons, but with a stronger zonal mean structure. Seager

et al. (2003) and L’Heureux and Thompson (2006) suggested that the extratropical response to tropical SST forcing in the austral summer yields a PSA-type wave train, but with a stronger zonal mean structure, which may further strengthen the variability of the annular SAM pattern in that season. We perform EOF analysis of the austral summer (NDJFM) SLP anomalies in the SH (90°–20°S) for the period 1921–2011. The structure of EOF1 closely resembles the SAM pattern, while the structure of EOF2 closely resembles the PSA1 pattern (not shown). The first principal component (PC1) associated with the EOF1 exhibits a correlation of 0.39 (significant at the 99.9 % level) with the MCA SLP expansion coefficient, which is lower than the correlation (0.63) between the PC2 and the MCA SLP expansion coefficient, lending support to the idea that this MCA SLP pattern preceding ENSO is more closely linked to the PSA1 pattern than the SAM pattern. Consequently, this MCA SLP pattern is hereafter referred to as the PSA pattern.

During the following austral summer, the Pacific SST is dominated by the developing and mature stages of ENSO, with positive anomalies in the eastern tropical Pacific and negative anomalies in the western tropical Pacific. These results confirm a robust lagged relationship between the PSA and ENSO, consistent with Jin and Kirtman (2009) and Ding et al. (2015b). Ding et al. (2015b) further suggested that the importance of the PSA in initiating ENSO events is comparable with that of the NPO. For the remainder of this study, we will use the time series associated with the MCA SLP and SST patterns to represent the PSA and ENSO indices, respectively, during the austral summer.

Despite the robustness of the interannual relationship between the austral summer(−1) PSA and the austral summer(0) ENSO for the entire period (1921–2011), we notice from Fig. 2c that their relationship is not stationary, and shows mostly in-phase variations during some decades, but mostly out-of-phase variations during other decades. To validate the secular evolution of the relationship between the PSA and ENSO, we show the sliding correlation between the austral summer(−1) PSA index and the austral summer(0) ENSO index in Fig. 3a. This shows that the PSA–ENSO relationship has undergone a distinct interdecadal variation, with significant positive correlations for the periods 1956–1975 and 1990–2004, but no significant (generally weak positive or even negative) correlations for 1928–1956 and 1975–1990. These results suggest that the influence of the PSA on ENSO may not always be strong, but varies considerably over interdecadal timescales, which is consistent with Ding et al. (2015b) who reported that the PSA–ENSO relationship experienced a marked weakening around the mid-1970s, followed by a sharp recovery in the early 1990s. Similar results can also be obtained

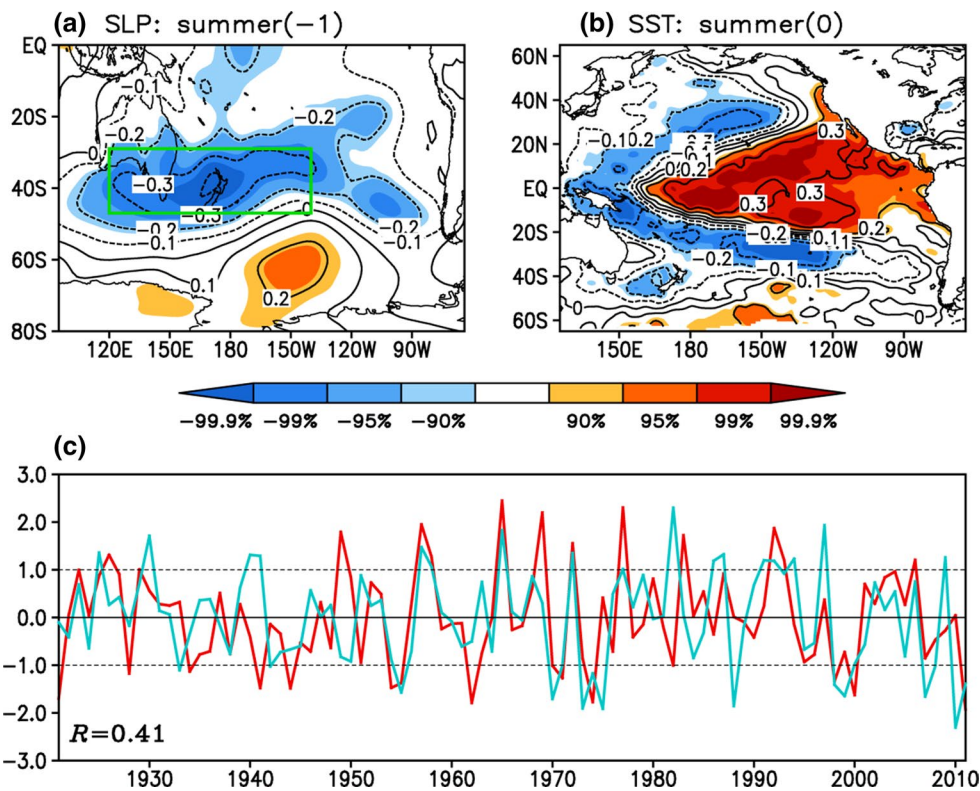


Fig. 2 Spatial properties of the leading MCA mode for **a** the austral summer(-1) (NDJFM-averaged) South Pacific (140°E – 68°W , 80° – 20°S) SLP anomalies and **b** the following austral summer(0) (ONDJF-averaged) tropical Pacific (125°E – 75°W , 20°S – 20°N) SSTAs, shown as correlation maps of the respective heterogeneous SLP and SST fields with the MCA leading normalized expansion coefficients. **c** The MCA leading normalized expansion coefficients

of the austral summer(-1) SLP field (red line) and the following austral summer(0) tropical Pacific SST field (light blue line). In **a**, **b**, areas with correlation significant at or above the 90 % level are shaded. In **a**, the region (120°E – 140°W , 47 – 29°S) of maximum SLP correlation is denoted by the green box. In **c**, the correlation between the two time series is given in the lower left corner, and the horizontal dashed lines indicate ± 1 standard deviation

when the PSA and ENSO indices are calculated from the MCA between the 20CRv2 SLP and ERSSTv3b SST data, or between the HadSLP2r SLP and HadISST SST data, and between the HadSLP2r SLP and ERSSTv3b SST data (Fig. 4). Figure 4 shows that the sliding correlations between the PSA and ENSO indices obtained using different SLP and SST dataset combinations bear a strong resemblance to each other, with correlation coefficients varying between 0.85 and 0.97 (Table 1), which provides increased confidence in these results. Hereafter, for convenience, the periods 1956–1975 and 1990–2004 are referred to as the high correlation (HC) periods (the HC1 and HC2 periods, respectively), whereas the periods 1928–1956 and 1975–1990 are referred to as the low correlation (LC) periods (the LC1 and LC2 periods, respectively).

Figure 5a–d shows the regressions of the austral summer(0) SSTAs on the austral summer(-1) PSA index for the four periods (i.e., LC1, HC1, LC2, and HC2). The regression SSTA patterns show remarkable differences between the HC and LC periods. During both HC1 and HC2, the central and eastern equatorial Pacific is

dominated by significant positive SSTAs, accompanied by significant negative SSTAs in the tropical western Pacific, which reflects the typical features of the El Niño peak phase (Fig. 5b, d). In contrast, during both LC1 and LC2, the austral summer PSA-associated SSTAs in the following austral summer are rather weak, and the El Niño-like regression pattern almost disappears (Fig. 5a, c). Furthermore, we compared the percentage of the El Niño (La Niña) events preceded by a positive (negative) PSA event for the four periods (Table 2). One El Niño or La Niña event is defined as a year when the ENSO index shown in Fig. 2c is greater than one standard deviation (SD) or less than one negative SD. One positive or negative PSA event is the same as the definition of an El Niño or La Niña event. We note that a high percentage (>50 %) of the El Niño (La Niña) events are preceded by a positive (negative) PSA event during both HC1 and HC2. In contrast, only a very low percentage (ca. 20 %) of the El Niño (La Niña) events are preceded by a positive (negative) PSA event during both LC1 and LC2. These results support the proposal that the connection between the austral summer PSA and

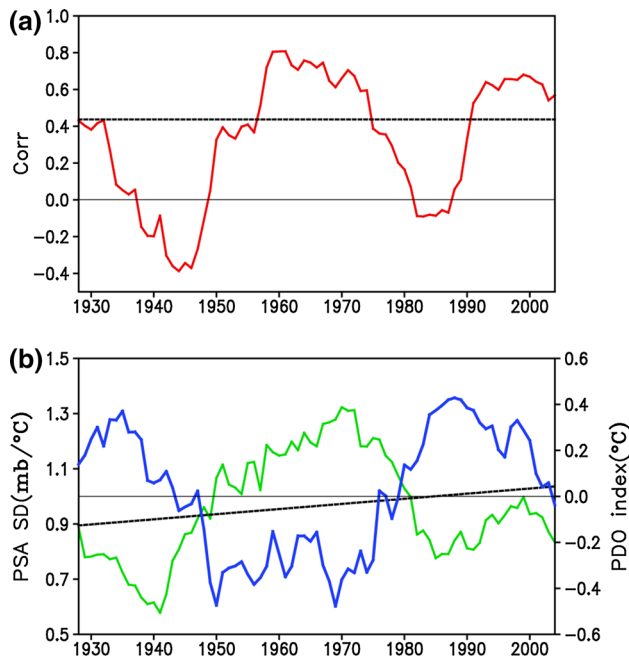


Fig. 3 **a** The 15-year sliding correlation between the austral summer(-1) PSA index and the austral summer(0) ENSO index for the period 1921–2011. The PSA and ENSO indices are calculated from the MCA between the 20CRv2 SLP and HadISST SST data. The horizontal dashed line shows the 90 % significance level. **b** The running SD of the austral summer PSA index (green line, scale on the left y-axis) and the running mean of the austral summer PDO index (blue line, scale on the right y-axis) calculated within a 15-year window that moves year-by-year for the period 1921–2011. The black dashed line indicates the linear trend of running SD of the austral summer PSA index

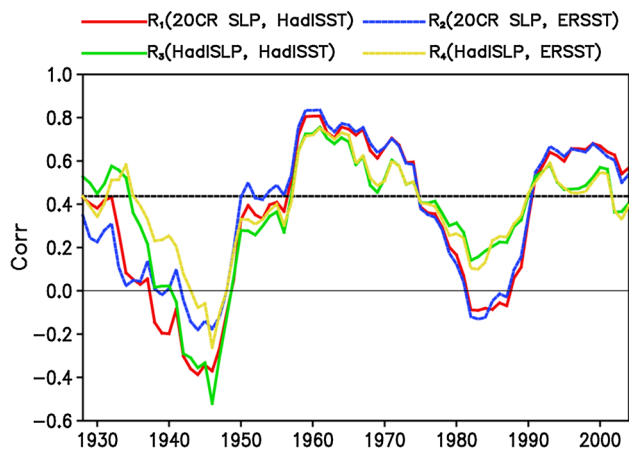


Fig. 4 The 15-year sliding correlation for various PSA and ENSO indices calculated using MCA between the 20CRv2 SLP and HadISST SST data (red line is same as Fig. 3a, denoted as R_1), the 20CRv2 SLP and ERSSTv3b SST data (blue line, R_2), the HadISLP SLP and HadISST SST data (green line, R_3), and the HadISLP2r SLP and ERSSTv3b SST data (yellow line, R_4). The horizontal dashed line shows the 90 % significance level

Table 1 Correlations between the time series of the four 15-year sliding correlations of PSA and ENSO indices in Fig. 4 (R_1 , R_2 , R_3 , R_4)

	R_1	R_2	R_3	R_4
R_1	—	0.97	0.90	0.89
R_2	—	—	0.85	0.87
R_3	—	—	—	0.96
R_4	—	—	—	—

All correlations are significant at or above the 95 % level

ENSO in the following austral summer tends to strengthen (weaken) during the HC (LC) periods.

4 Changes in the PSA-related atmospheric and oceanic anomalies during the HC and LC periods

Why does the austral summer PSA exhibit a strengthened relationship with the following austral summer ENSO during the HC periods, but this relationship breaks down during the LC periods? To address this question, it is necessary to examine whether the processes through which the austral summer PSA triggers the onset of the following austral summer ENSO are significantly different during the HC and LC periods. According to Ding et al. (2015b), the austral summer PSA can trigger the onset of the following austral summer ENSO via the following two dominant processes: (1) coupling between SST and surface wind stress associated with the PSA in the subtropical/tropical Pacific, which resembles the SFM (Vimont et al. 2003a, b); and (2) evolution of subsurface ocean temperature anomalies along the equator associated with the PSA, which resembles the TWC (Anderson 2004; Anderson et al. 2013). In this section, we examine in detail the evolution of the austral summer PSA-related SST, surface wind, and subsurface ocean temperature anomalies during the HC and LC periods, with the aim of identifying whether both processes of surface air–sea coupling and subsurface ocean temperature evolution associated with the PSA are significantly different during the HC and LC periods.

We first examine, in Fig. 6, the spatial patterns of the 3-month averaged SST and surface wind anomalies correlated with the austral summer(-1) (NDJFM-averaged) PSA index for a range of time lags during the HC (left panel) and LC (right panel) periods. During the HC periods (1956–1975 and 1990–2004), we note that anomalous surface winds associated with the PSA force a notable quadrupole-like SSTA pattern in the extratropical South Pacific during

Fig. 5 Regressions of the austral summer(0) (ONDJF-averaged) SSTAs (contour interval 0.2°C) on the austral summer(−1) (NDJFM-averaged) PSA index for the **a** LC1 (1928–1956), **b** HC1 (1956–1975), **c** LC2 (1975–1990), and **d** HC2 (1990–2004) periods. Positive (red) and negative (blue) SSTAs, significant at the 90 % level, are shaded

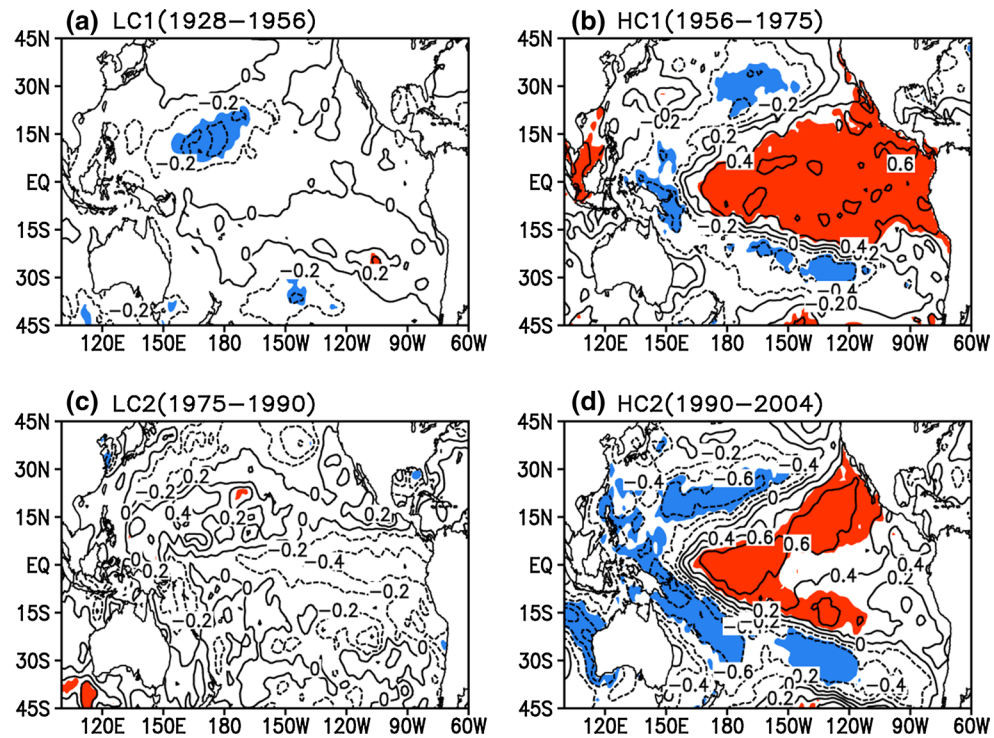


Table 2 Percentage of El Niño (La Niña) events preceded by a positive (negative) PSA event for the LC1, HC1, LC2, and HC2 periods

LC1	HC1	LC2	HC2
17 %	78 %	20 %	50 %

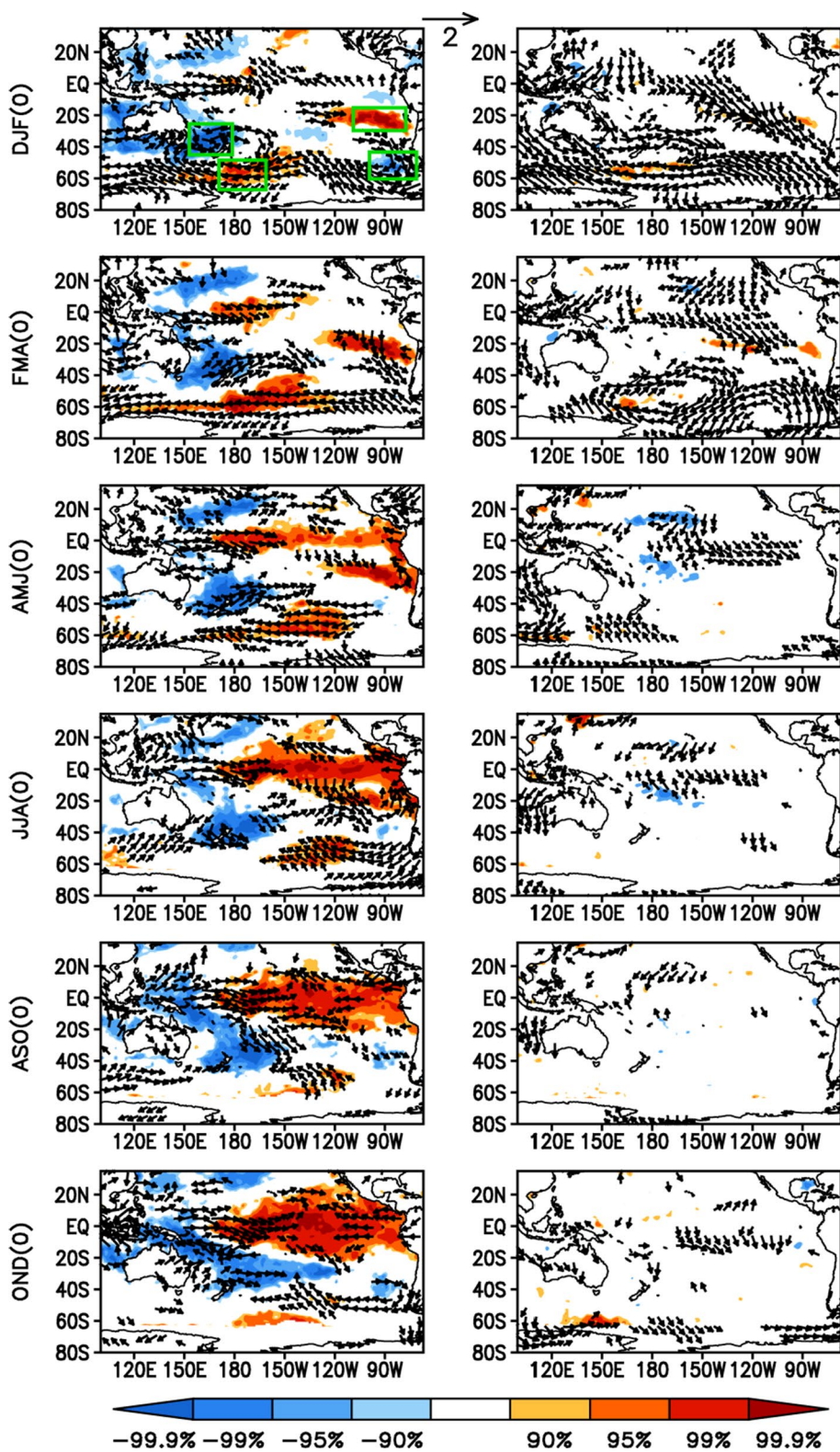
DJF(0). As suggested by Ding et al. (2015b), although the PSA patterns in the SH are weakest during the austral summer when ENSO tends to reach its peak, the SST footprint forced by the PSA in the South Pacific (i.e., a quadrupole-like SSTA pattern) is strongest because of the influence of the seasonal variations in the ocean mixed layer depth [MLD; see Ding et al. (2015b) for more details].

During DJF(0), we can also see that westerly wind anomalies associated with the PSA occur in the western-central equatorial Pacific, which can favor the development of positive SSTAs in the central equatorial Pacific. The quadrupole-like SSTA pattern (mainly its related subtropical portion) can persist into the following austral late autumn and early winter [AMJ(0)] through the positive WES feedback (Xie and Philander 1994) and can subsequently force the overlying atmosphere, resulting in westerly wind anomalies along the equator that tend to strengthen anomalous westerlies in the western-central equatorial Pacific associated with the PSA. The strengthened anomalous westerlies there act to further develop the initial warming in the central–eastern equatorial Pacific. After JJA(0), air-sea interaction through a

positive feedback process (i.e., the Bjerknes feedback) in turn amplifies the zonal wind and SST anomalies along the equator (Bjerknes 1969). This positive feedback process drives continued growth of zonal wind and SST anomalies. During OND(0), and lagging the austral summer(−1) PSA signal by about 10 months, a PSA-related warming pattern becomes well established in the central–eastern equatorial Pacific. The evolution of the PSA-related SST and surface wind anomalies described above are generally similar to those obtained by Ding et al. (2015b) using the reanalysis data for the period 1950–2011.

In contrast, during the LC periods (1928–1956 and 1975–1990) the PSA-related SSTAs in the extratropical South Pacific are very weak, and the quadrupole-like SSTA pattern becomes indistinct during DJF(0). As a result, westerly wind anomalies do not develop in the western–central equatorial Pacific during the following austral winter, and the warming in the central–eastern equatorial Pacific does not occur until OND(0). The large contrast in the correlation of variability of the PSA-forced quadrupole-like SSTA pattern during DJF(0) with the austral summer(−1) PSA index between the HC and LC periods can be more clearly seen in Table 3. Variability of the PSA-forced quadrupole-like SSTA pattern is measured by the difference between the sum of the normalized SSTAs averaged within the two boxes where strong positive correlations are seen in the top left panel of Fig. 6, and the sum of the normalized SSTAs averaged within the other two boxes where strong negative correlations are seen in the top left panel of Fig. 6.

Fig. 6 Correlation maps of the 3-month averaged SST and surface wind anomalies correlated with the austral summer (−1) (NDJFM-averaged) PSA index for DJF(0), FMA(0), AMJ(0), JJA(0), ASO(0), and OND(0) during the HC (left panel) and LC (right panel) periods. Positive (red) and negative (blue) SSTAs, with correlation significant at or above the 90 % level, are shaded. Only surface wind vectors significant at the 90 % level are shown. In the top left panel, four green boxes [from left to right: (153°–178°E, 45°–25°S); (170°E–161°W, 67°–48°S); (103°–76°W, 30°–15°S); and (109°–78°W, 60°–43°S)] define the locations of the four poles of the PSA-forced quadrupole-like SSTA pattern



According to the above analysis, the connection between the PSA-like SLP anomalies and ENSO involves the development of ENSO in response to surface zonal wind anomalies along the equator associated with the PSA. To further

illustrate the differences in the temporal evolution of the PSA-related surface zonal wind anomalies along the equator and ENSO between the HC and LC periods, Fig. 7a and b shows the lead–lag regression coefficients of the 3-month

Table 3 Correlation of variability of the PSA-forced quadrupole-like SSTA pattern during DJF(0) with the austral summer(−1) PSA index for the LC1, HC1, LC2, and HC2 periods

LC1	HC1	LC2	HC2
0.37*	0.87***	0.44	0.71**

* Correlation significant at the 95 % level

** Correlation significant at the 99 % level

*** Correlation significant at the 99.9 % level

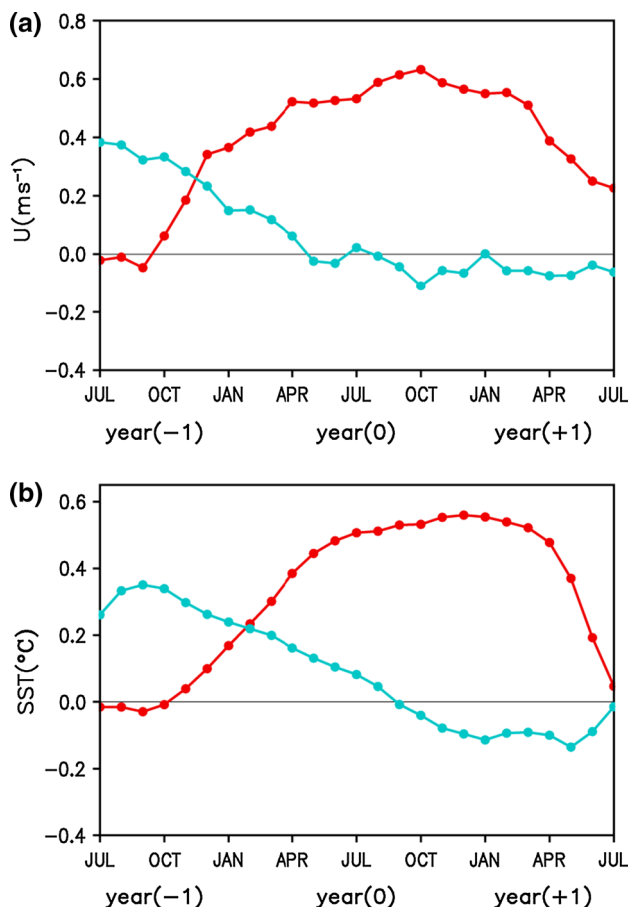


Fig. 7 Lead-lag regression coefficients of the 3-month running mean **a** surface zonal wind anomalies averaged over the western-central equatorial Pacific (150°E – 160°W , 5°S – 5°N) and **b** Niño3.4 index on the austral summer(−1) PSA index for the HC (red line with dots) and LC (blue line with dots) periods. The ENSO-developing year is denoted as year(0) and the preceding and following years as year(−1) and year(+1), respectively

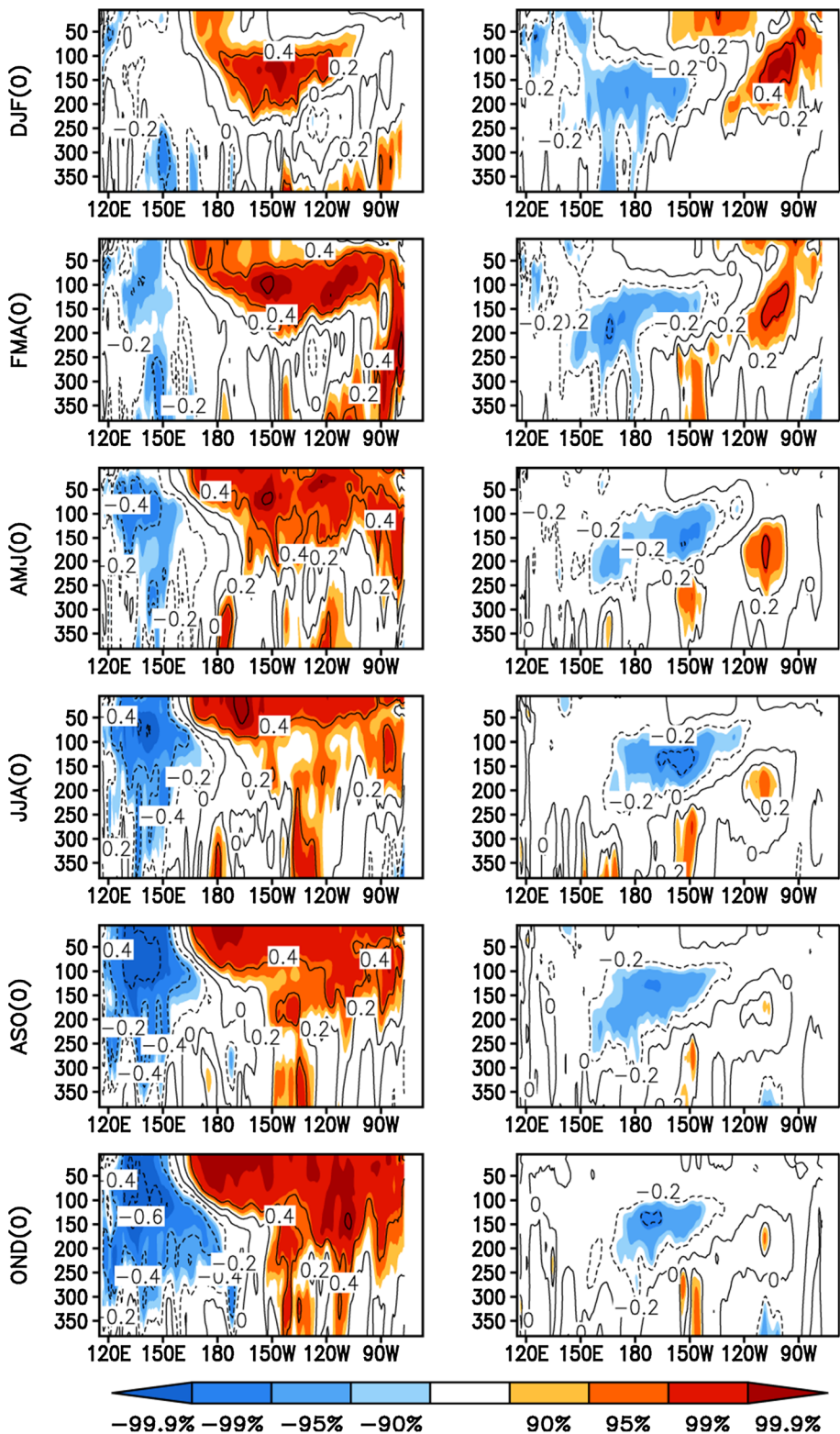
running mean surface zonal wind anomalies averaged over the western-central equatorial Pacific (150°E – 160°W , 5°S – 5°N) and Niño3.4 index [defined as SST averaged over (170° – 120°W , 5°S – 5°N)] on the austral summer(−1) PSA index for both periods. We can see that for the HC periods, westerly wind anomalies occur in the western-central

Pacific along the equator during the austral summer(−1), then gradually intensify during the austral autumn(0) and winter(0), and reach a peak during the austral summer(0). In contrast, for the LC periods, westerly wind anomalies are seen in the western-central equatorial Pacific during the austral summer(−1), but they gradually decay and vanish during the austral autumn(0) and winter(0) (Fig. 7a). The evolution of the Niño3.4 index is consistent with that of the westerly wind anomalies along the equator for both the HC and LC periods. During the HC periods, the Niño3.4 index is relatively weak during the austral summer(−1), intensifies almost in phase with westerly wind anomalies along the equator during the austral autumn(0) and winter(0), and reaches a maximum during the austral summer(0). During the LC periods, however, the Niño3.4 index gradually decreases to reach a small negative value during the austral summer(0) (Fig. 7b).

We further compared the evolution of the 3-month averaged subsurface ocean temperature anomalies correlated with the austral summer(−1) PSA index during the HC and LC periods (Fig. 8). During the HC periods, significant positive subsurface temperature anomalies appear in the central equatorial Pacific (between 175°E and 120°W) at around 100–250 m depth during DJF(0). According to the TWC mechanism (Anderson 2004; Anderson et al. 2013), these positive subsurface ocean temperature anomalies are most probably generated along the equator by surface wind anomalies associated with the PSA. After FMA(0), they propagate eastwards and upwards along the subsurface pycnoclines, and reach the eastern equatorial Pacific during JJA(0), where they start to strengthen the surface warming. During the LC periods, however, no obvious propagation of the austral summer(−1) PSA-related positive subsurface ocean temperature anomalies can be seen in the central–eastern equatorial Pacific; instead, negative subsurface ocean temperature anomalies, initially in the western–central equatorial Pacific at around 150–300 m depth, show a well-defined eastwards and upwards propagation, and reach the near-surface layer in the eastern equatorial Pacific during JJA(0), which is less favorable for the development of surface warming there.

The results presented above indicate that the evolution of the austral summer PSA-related SST, surface wind, and subsurface ocean temperature anomalies along the equator differ significantly during the HC and LC periods. The influence of the austral summer PSA on the extratropical/tropical South Pacific SST and surface wind anomalies in the following austral winter are strong enough to trigger ENSO events during the HC periods, whereas these influences are too weak to trigger ENSO events during the LC periods. This implies that changes in the intensity of the austral summer PSA-related SST and surface wind anomalies in the extratropical/tropical South Pacific may play an

Fig. 8 Correlation maps of the 3-month averaged subsurface ocean temperature anomalies with the austral summer (−1) (NDJFM-averaged) PSA index for DJF(0), FMA(0), AMJ(0), JJA(0), ASO(0), and OND(0) during the HC (left panel) and LC (right panel) periods. Positive (red) and negative (blue) subsurface ocean temperature anomalies, with correlation significant at or above the 90 % level, are shaded



important role in the PSA–ENSO relationship. Additionally, the evolution of subsurface ocean temperature anomalies along the equator associated with the austral summer PSA is less favorable for the development of surface

warming in the eastern equatorial Pacific during the LC periods, which may also be closely linked to the evolution of the austral summer PSA-related westerly wind anomalies along the equator.

5 Possible causes of the changes in the PSA–ENSO relationship

Our results demonstrate that there are significant differences in the intensity of the austral summer PSA-related SST and surface wind anomalies in the extratropical/tropical South Pacific between the HC and LC periods. However, the question of what caused these differences between the two periods remains. As mentioned in the introduction, the ENSO teleconnection to the high-latitude South Pacific, namely the PSA pattern, has been shown to exhibit decadal variability (e.g., Wang and Ropelewski 1995; Wang and Wang 1996; Gershunov and Barnett 1998; McCabe and Dettinger 1999; Mann et al. 2000; Hunt and Elliott 2003; Power et al. 2006). In view of the marked effect of the austral summer PSA on the SST and surface wind anomalies in the extratropical/tropical Pacific during subsequent seasons, it is of interest to explore whether it is the change in the intensity of the austral summer PSA itself that is responsible for the decadal change in the PSA–ENSO relationship.

Figure 3b shows the 15-year running SD of the austral summer PSA index for the period 1921–2011. The interannual variability of the austral summer PSA index exhibits a marked decadal change, with the lowest SD from the late 1920s to the early 1950s, and the highest SD from the early 1950s to the late 1970s. Afterwards the SD experiences a marked weakening in the 1980s, followed by a slight increase in the 1990s. We note that the intensity of the austral summer PSA fluctuates almost in phase with its relationship with ENSO shown in Fig. 3a. Comparison of the correlation time series in Fig. 3a and the running SD in Fig. 3b yields a HC of 0.69 (significant at the 95 % level). This implies that a stronger PSA generally corresponds to a strengthened relationship between the PSA and ENSO during the HC periods; in contrast, a weaker PSA generally corresponds to a weakened relationship between the PSA and ENSO during the LC periods. These results, combined with those presented above, suggest that a stronger (weaker) PSA in the austral summer tends to exert a stronger (weaker) influence on the subsequent SST and surface wind anomalies in the extratropical/tropical Pacific and hence ENSO. Similar results have also been obtained for the North Pacific, where decadal variations of the extratropical forcing are found to be generally consistent with its relationship with ENSO, as shown in Ding et al. (2015a; Fig. 12).

Next we examine two possible mechanisms to explain the decadal changes in the intensity of the austral summer PSA presented above. The first mechanism proposed is that the Pacific decadal oscillation (PDO)/interdecadal Pacific oscillation (IPO) may exert a modulating effect on the ENSO teleconnection in the South Pacific. It is well

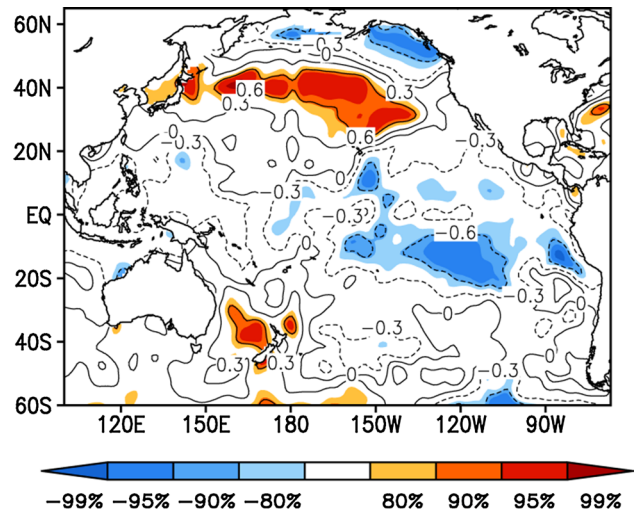


Fig. 9 Correlation map of the 15-year running SD of the austral summer (NDJFM-averaged) PSA index in Fig. 3b with the 15-year running mean of the austral summer SSTAs. Positive (red) and negative (blue) SSTAs, with correlation significant at or above the 80 % level, are shaded

known that the PDO is an El Niño-like pattern of North Pacific climate variability, oscillating between its warm and cool phase about every 20–30 years (Mantua et al. 1997; Zhang et al. 1997). The extension of the PDO to the whole Pacific basin is known as the IPO (Power et al. 1999). The PDO and IPO exhibit almost similar temporal evolution on annual and longer time scales. Many studies have revealed that the PDO/IPO modulates the climatic impacts of ENSO over many parts of the world, such as East Asia (Wang et al. 2008; Kim et al. 2013), North America (Gershunov and Barnett 1998; Gutzler et al. 2002; Hu and Huang 2009), South America (Andreoli and Kayano 2005; Pavia et al. 2006), and Australia (Power et al. 1999; Arblaster et al. 2002). Figure 9 shows the correlations of the 15-year running SD of the austral summer PSA index in Fig. 3b with the 15-year running mean of the austral summer SSTAs. There are significant negative correlations in the tropical eastern Pacific, coincident with significant positive correlations in the central North Pacific and negative correlations in the Gulf of Alaska, closely resembling the spatial pattern of the cold PDO/IPO phase in the North Pacific (Mantua et al. 1997; Zhang et al. 1997; Power et al. 1999). Furthermore, it is noted that there is a strong out-of-phase relationship between the 15-year running SD of the austral summer PSA index and the 15-year running mean of the austral summer PDO index (Fig. 3b); the latter is defined as the PC1 time series associated with the EOF1 of SSTAs in the North Pacific poleward of 20°N. The two time series are highly anti-correlated at a value of −0.73 (significant at the 95 % level), such that warm (cold) PDO phases are

generally associated with the weakened (strengthened) PSA pattern.

The physical processes that are responsible for the modulation of the PDO/IPO on the ENSO teleconnections have been extensively discussed in the literature. Arblaster et al. (2002) suggested that the PDO/IPO could exert a direct modulation on the characteristics of ENSO, including changes to the frequency, seasonality, spatial patterns, intensity, and the three-dimension structure of El Niño and La Niña events. They found that the observed ENSO amplitude is weakened by the deepening of the thermocline in the eastern Pacific during warm PDO phases (see their Table 1), possibly leading to a weaker influence on the Australian climate. Nevertheless, we calculate the 15-year running SD of the austral summer (NDJFM) Niño3.4 index (not shown). We note that decadal variations in the ENSO intensity do not fluctuate in phase with those in the PSA–ENSO relationship shown in Fig. 3a, and the two time series have a low correlation of 0.25, indicating that decadal variations in the PSA–ENSO relationship may be not simply a result of the decadal variations in the ENSO intensity. In addition to the influence of the PDO on the ENSO amplitude, some studies suggest that the shift of the PDO from one phase to another is generally associated with a shift in the positions of the Walker circulation and associated convection (Power et al. 1999; Arblaster et al. 2002; Andreoli and Kayano 2005). Ding et al. (2012) reported that the PSA pattern is very sensitive to small variations in tropical convection. It thus appears that shifts in the position of the Walker circulation associated with the PDO may be another physical process that contributes to the differences in PSA intensity between different phases of the PDO.

Figure 10a, b shows the correlation of the austral summer (NDJFM-averaged) 500 hPa GHT anomalies with the austral summer SOI during warm and cold PDO phases. As expected, the correlation maps show substantial differences between warm and cold PDO phases. Notably, there are significant positive correlations across a much larger region in the mid-latitude South Pacific during the cold PDO phase than during the warm PDO phase. Moreover, the maximum negative correlation is located near 60°S, 140°W during the cold PDO phase, but shifts east during the warm PDO phase, placing the maximum along the Bellinghausen Sea–Antarctic Peninsula coastline. The pattern of the difference in correlations between cold and warm PDO phases in the South Pacific (Fig. 10c) closely resembles the PSA pattern shown in Fig. 2b, suggesting that the PSA pattern is weaker during the warm PDO phase than during the cold PDO phase.

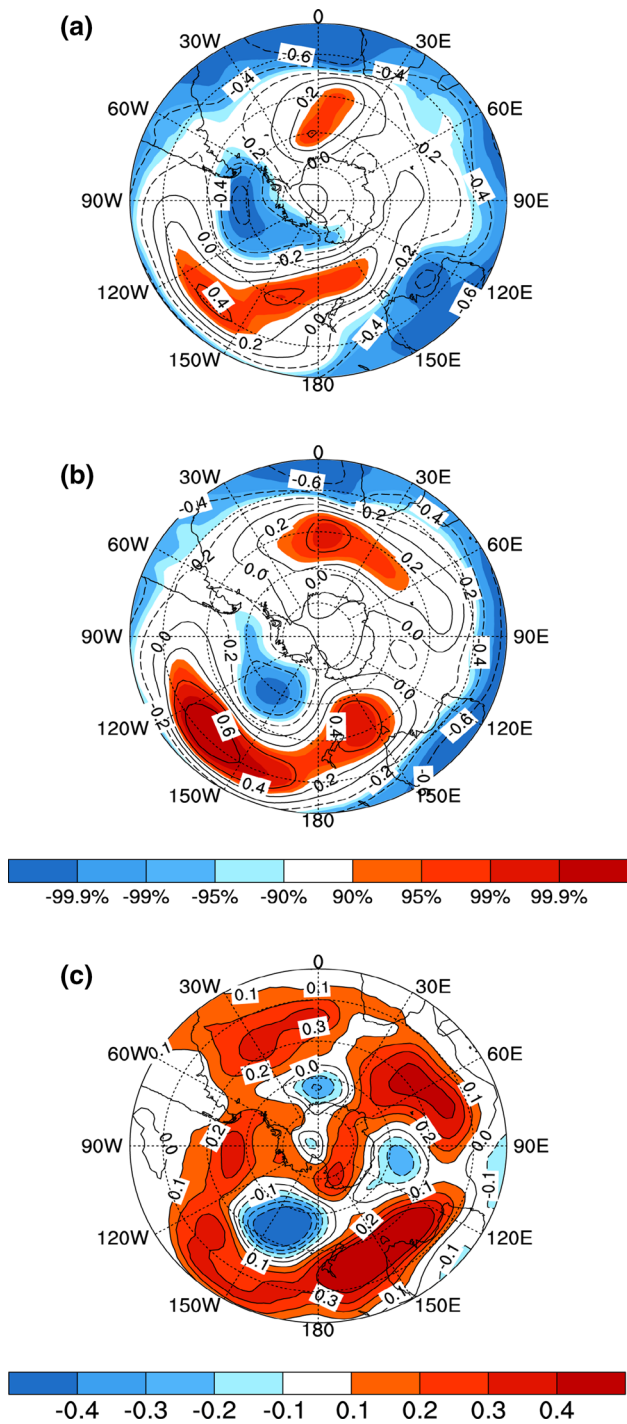


Fig. 10 **a** Correlation map of the austral summer (NDJFM-averaged) 500 hPa GHT anomalies with the austral summer SOI during the warm PDO phase (1928–1943 and 1980–1998; see Fig. 3b). Positive (red) and negative (blue) GHT anomalies, with correlation significant at or above the 90 % level, are shaded. **b** As **a**, but for the cold PDO phase (1945–1979). **c** The difference between **b** and **a**. contour interval is 0.1; differences >0.1 or <-0.1 are shaded

To better understand the underlying dynamics of the relatively weak (strong) PSA pattern during the warm (cold) PDO phase, we calculated the NDJFM-averaged Rossby wave source (RWS) at 200 hPa during warm and cold PDO phases, respectively. The RWS (denoted as S) is defined as

$$S = -\mathbf{v}_x \cdot \nabla \zeta - \zeta D, \quad (2)$$

where \mathbf{v}_x is the divergent component of velocity, ζ is the vertical component of the absolute vorticity, and D is the divergence (Sardeshmukh and Hoskins 1988; Shimizu and Cavalcanti 2011). According to Ding et al. (2012), the PSA pattern, as a tropically forced Rossby wave train, is related to an active RWS region along the subtropical jet with a maximum to the east of Australia. Figure 11a shows the correlation of the austral summer (NDJFM-averaged) 200 hPa RWS anomalies with the austral summer PSA index. We can see that there are significant positive correlations to the east of Australia where the RWS is most active (i.e., with the strongest year-to-year variability), consistent with the findings of Ding et al. (2012). Composite difference of the SD of the austral summer RWS between cold and warm ENSO phases (cold minus warm) using 20CRv2, as shown in Fig. 11b, indicates that the RWS SD becomes stronger in the active RWS region to the east of Australia during the cold PDO phase than during the warm PDO phase. The differences of RWS activity to the east of Australia between the cold and warm PDO phases obtained from the NCEP1 reanalysis data (not shown) are very similar to those from 20CRv2. These results indicate that the PDO does modulate the RWS activity to the east of Australia; the latter may in turn influence the intensity of the PSA pattern. The weaker RWS to the east of Australia during the warm PDO phase may be attributed to the impacts of both the weakened ENSO amplitude and shifts in the position of the Walker circulation, as noted previously (Power et al. 1999; Arblaster et al. 2002).

The second mechanism responsible for the decadal changes in the intensity of the austral summer PSA is that long-term variability in the SAM may act to modulate the mean interdecadal intensity of the PSA pattern. As noted by previous studies (Fogt and Bromwich 2006; Ding et al. 2012), both the PSA and SAM patterns have large loading centers in the South Pacific and Amundsen–Bellingshausen Seas region. The spatial overlap of these loading centers indicates that the SAM can contribute to the variability of the PSA and vice versa. Recent studies have reported that the austral summer SAM has exhibited long-term trends over the past few decades towards positive polarity during the austral summer, which has been attributed not solely to stratospheric ozone depletion but also to anthropogenic and natural climate variability, including the variability in the tropical Pacific SSTAs (Thompson and Solomon 2002; Gillett and Thompson 2003; Marshall et al. 2004; Arblaster

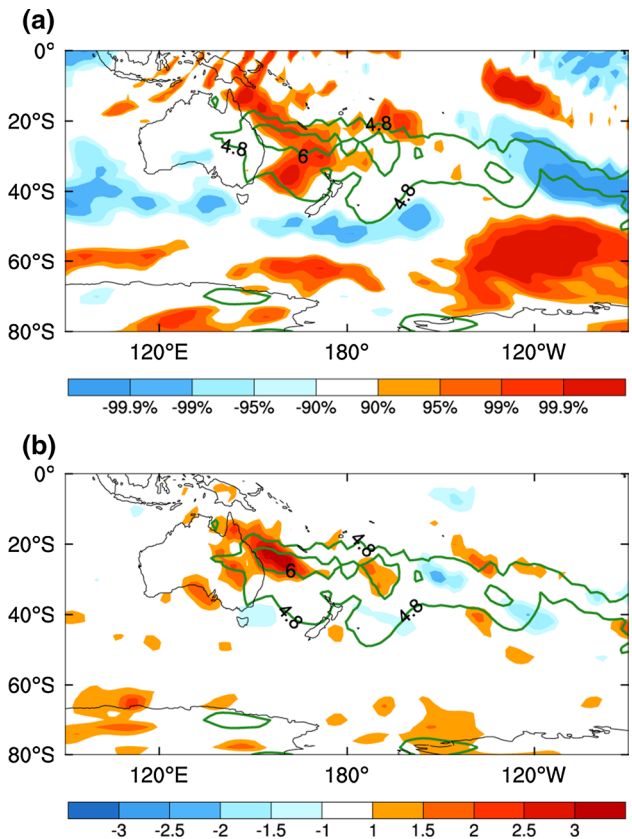
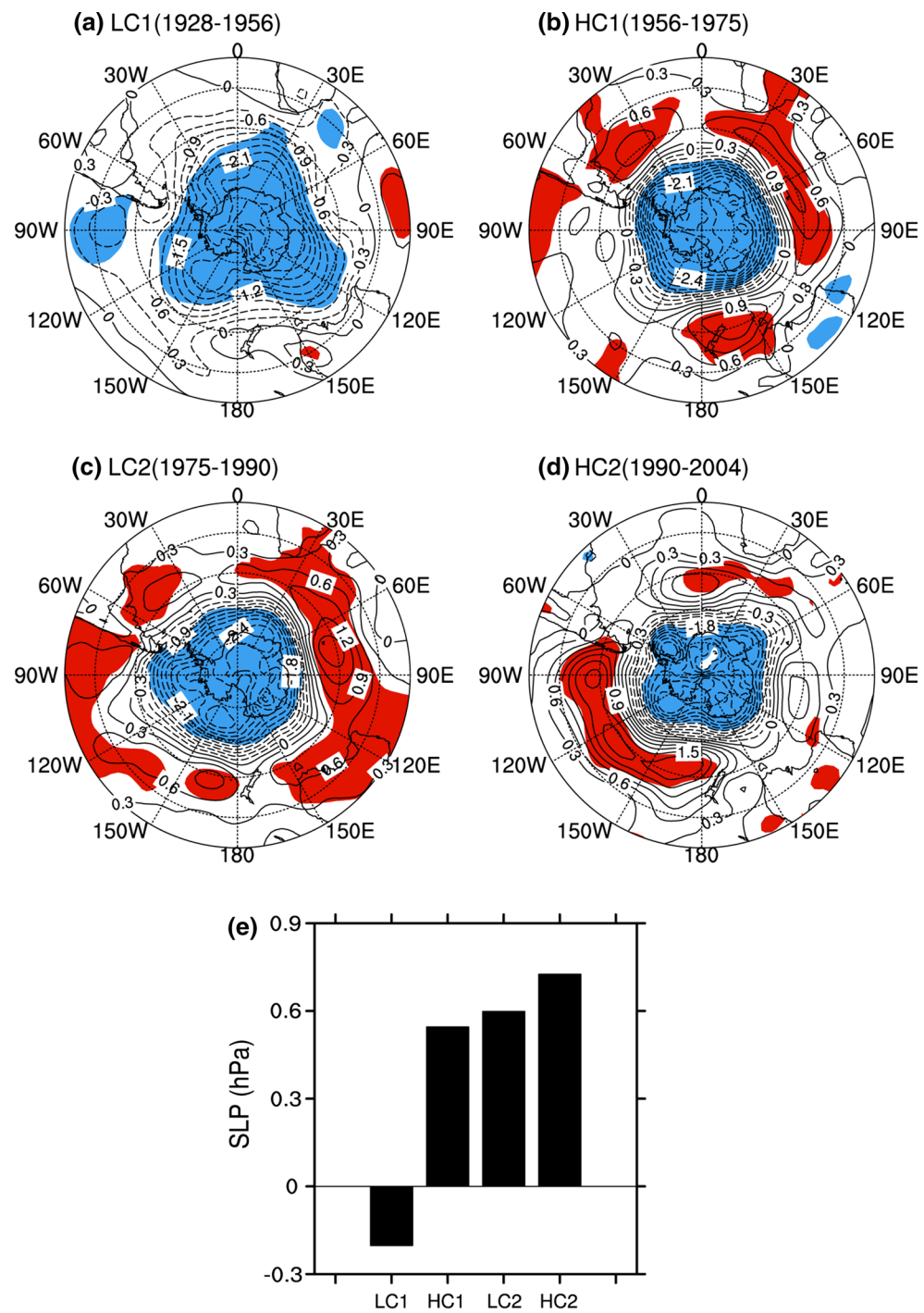


Fig. 11 **a** Correlation map of the austral summer (NDJFM-averaged) 200 hPa RWS anomalies with the austral summer PSA index for the period 1921–2011. Positive (red) and negative (blue) RWS anomalies, with correlation significant at or above the 90 % level, are shaded. **b** Composite difference of the SD of the austral summer RWS (shading, unit 10^{-11} s^{-2}) between cold and warm ENSO phases (cold – warm). In **a** and **b**, the climatological (1921–2011) SD of the austral summer RWS is superposed as green contours ($1.2 10^{-11} \text{ s}^{-2}$ contour interval, values $>4.8 10^{-11} \text{ s}^{-2}$ only)

and Meehl 2006; Ding et al. 2012). It is speculated that long-term variability in the SAM may influence the mean interdecadal intensity of the PSA pattern through its projection onto the pressure anomalies in the South Pacific. To verify this speculation, we calculated the regressions of the austral summer SLP anomalies on the austral summer SAM index for LC1, HC1, LC2, and HC2 (Fig. 12a–d). The SAM index is defined as the PC1 time series associated with the EOF1 of SLP anomalies in the SH poleward of 20°S . According to Ding et al. (2012), the SAM index derived from SLP anomalies is highly correlated with that derived from the 500 hPa GHT anomalies. Prior to the regression analysis, the austral summer Niño3.4 index was linearly removed from the austral summer SLP anomalies. The removal of the austral summer Niño3.4 index from the data ensures that the austral summer SLP anomalies are independent of any ENSO variability that occurs simultaneously in the tropical Pacific.

Fig. 12 Regressions of the austral summer (NDJFM-averaged) SLP anomalies (contour interval 0.3 hPa) on the austral summer SAM index for the **a** LC1 (1928–1956), **b** HC1 (1956–1975), **c** LC2 (1975–1990), and **d** HC2 (1990–2004) periods. Positive (red) and negative (blue) SLP anomalies, significant at the 90 % level, are shaded. **e** SLP anomalies (with sign reversed) regressed on the SAM index, as shown in **(a)**–**(d)**, averaged over the region of maximum SLP correlation with ENSO 1 year later (denoted by the green box in Fig. 2a) for LC1, HC1, LC2, and HC2



It is evident that during HC2, both the austral summer SAM-related positive and negative SLP anomalies are strongest in the mid- and high-latitudes of the South Pacific, respectively, thereby exhibiting a pronounced dipole structure in the South Pacific sector (Fig. 12d); in contrast, during LC1, these positive and negative SLP anomalies (especially positive SLP anomalies) associated with the austral summer SAM are weakest in the South Pacific sector, leading to an indistinct dipole pattern there

(Fig. 12a). The strongest SAM-related SLP anomalies in the South Pacific sector during the HC2 period are consistent with the strengthened SAM in recent decades. During both the HC1 and LC2 periods (Fig. 12b, c), the austral summer SAM-related SLP anomalies in the South Pacific sector are weaker than those during HC2, but stronger than those during LC1. Note that, although the amplitudes of the SAM-related SLP anomalies during HC1 and LC2 are generally comparable, the positions of the large SLP

anomalies differ in the two periods, which may lead to a slight difference in the projection of the SAM-related SLP anomalies on the PSA pattern. Furthermore, we calculated the SLP anomalies regressed on the SAM index shown in Fig. 12a–d averaged over the region of maximum SLP correlation with ENSO 1 year later (denoted by the green box in Fig. 2a) for HC1, LC1, HC2, and LC2. The area-averaged regressed SLP anomaly is largest during HC2, followed by LC2 and HC1, and finally LC1, showing an upward trend over time that is almost in accordance with the rise in the PSA intensity shown in Fig. 3b. These results suggest that, along with the long-term trend of the SAM, the projections of the SAM on the PSA pattern also contains substantial long-term variability, which may contribute to the interdecadal changes in PSA intensity.

It should be noted that, although our results suggest that the decadal changes in the intensity of the austral summer PSA are modulated by the PDO/IPO and long-term variations in the SAM, we do not exclude other possible mechanisms involving tropical–extratropical interactions that act to modulate the changes in the intensity of the PSA pattern. Fogt and Bromwich (2006) reported that the intensity of the ENSO teleconnection to the high-latitude South Pacific might be modulated by coupling of the SAM and ENSO (represented by their in-phase or out-of-phase relationship). They found that the ENSO teleconnection during September–November (SON) in the 1980s was weak because of interference between the SAM and ENSO, but an in-phase relationship between them during SON in the 1990s strengthened the ENSO teleconnection in the South Pacific. A recent study by Yu et al. (2015) suggested that the PSA and SAM tend to show more in-phase fluctuations in SON after the early-1990s. Also, in addition to the North and South Pacific extratropical forcings (i.e., the NPO and PSA) that may force the onset of ENSO events, some tropical phenomena, such as the Madden–Julian oscillation (MJO; Madden and Julian 1994) and westerly wind bursts (WWBs; McPhaden et al. 1992; McPhaden 1999), have been shown to play an important role in triggering the onset of ENSO events. It is very likely that these tropical effects of the MJO and WWBs on ENSO may counteract the extratropical effects of the PSA on ENSO in some decades but strengthen it in others, thereby modulating either the strengthened or weakened PSA–ENSO relationship over interdecadal timescales. Further research is necessary to examine the roles of these tropical–extratropical interactions in modulating the intensity, and hence impact, of the PSA pattern by using sufficiently realistic models.

In addition, Sun et al. (2015) suggested that the Atlantic multidecadal variability (AMV) is closely linked to the SH atmospheric circulation over decadal timescales. They showed that the Atlantic meridional overturning circulation (AMOC) can influence an anomalous anticyclone to the

southeast of Australia; the latter has potential to project on the PSA pattern, as shown in the green box of Fig. 2a, and the AMV may therefore modulate the decadal variations in the PSA intensity through its influence on the anomalous anticyclone to the southeast of Australia. The AMV shows a strong positive phase since the 1990s (Sun et al. 2015), which is in accordance with the strengthened PSA intensity for this period, suggesting a possible contribution of the AMV to the decadal variations in the PSA intensity. Further work is required to examine to what extent the AMV can influence the intensity of the PSA pattern over decadal timescales.

6 Summary and concluding remarks

Previous studies have suggested that the austral summer PSA-like atmospheric variability can influence the occurrence of ENSO events during the following austral summer. The present study indicates that the PSA–ENSO relationship has experienced a significant interdecadal change, with significant positive correlations over the periods 1956–1975 and 1990–2004, but no significant (generally weak positive or even negative) correlations for 1928–1956 and 1975–1990. These results suggest that the influence of the PSA on the subsequent ENSO is strong during the HC periods (1956–1975 and 1990–2004), but weak during the LC periods (1928–1956 and 1975–1990).

Two processes by which the PSA influences the subsequent ENSO involve the surface air–sea coupling and subsurface ocean temperature evolution associated with the PSA. By comparing these two processes in the HC and LC periods, we find that during the HC periods, the austral summer PSA is simultaneously associated with a remarkable quadrupole-like SSTA pattern in the extratropical South Pacific and significant westerly wind anomalies in the western–central equatorial Pacific, and the latter generates the initial warming in the central equatorial Pacific. The quadrupole-like SSTA pattern (mainly its related subtropical portion) can persist into the following austral winter and can subsequently force the overlying atmosphere, resulting in westerly wind anomalies along the equator that tend to strengthen anomalous westerlies in the western–central equatorial Pacific associated with the PSA. The strengthened anomalous westerlies along the equator then act to further develop the warming in the central–eastern equatorial Pacific. Consistent with westerly wind anomalies along the equator associated with the PSA during the austral summer, significant positive subsurface temperature anomalies occur in the central equatorial Pacific at around 100–250 m depth at the same time. Afterwards they propagate eastwards and upwards, and reach the eastern equatorial Pacific during the following austral winter where they

start to strengthen the surface warming there. Finally, these two processes may generate sufficient surface warming in the central–eastern equatorial Pacific to trigger an El Niño event. In contrast, during the LC periods, both processes of surface air–sea coupling in the extratropical/tropical Pacific and subsurface ocean temperature evolution along the equator are rather weak, and the warming in the central–eastern equatorial Pacific does not develop until the following austral summer, thereby leading to a weakened PSA–ENSO relationship during these periods.

We found that decadal changes in the intensity of the austral summer PSA are closely related to those of the PSA–ENSO relationship. The amplitude of the austral summer PSA is generally greater during the HC periods than during the LC periods. We concluded that the stronger (weaker) austral summer PSA during the HC (LC) periods tends to exert a stronger (weaker) influence on the subsequent SST and surface wind anomalies in the extratropical/tropical Pacific and finally on ENSO. We have demonstrated that changes in the intensity of the austral summer PSA are driven mainly by contributions from both the modulation of the PDO/IPO and long-term variations in the SAM. The PDO/IPO may exert a modulating effect on PSA intensity, possibly through its influence on the RWS activity to the east of Australia, whereas long-term variability in the SAM may influence the mean interdecadal intensity of the PSA pattern through its projection onto the pressure anomalies in the South Pacific.

It is worth noting that the spatial coverage of observations is poor before 1950, especially in the SH and in the equatorial Pacific (Ishii et al. 2005). We cannot entirely rule out the possibility that changes in the PSA–ENSO relationship are an artifact of changes in data coverage. However, the results presented here indicate that there is reasonably good agreement across the datasets currently available, which increases confidence in our findings. Nonetheless, the robustness of the results should be tested further.

Acknowledgments This research was jointly supported by the China Special Fund for Meteorological Research in the Public Interest (GYHY201306031), the 973 project of China (2012CB955200), the National Natural Science Foundation of China (41175069), and the Strategic Priority Research Program of the Chinese Academy of Sciences (XDA11010303). K.-J. Ha and J.Y. Lee were supported by the Global Research Laboratory (GRL) program from the National Research Foundation of Korea (Grant No. 2011-0021927).

References

Alexander MA, Vimont DJ, Chang P, Scott JD (2010) The impact of extratropical atmospheric variability on ENSO: testing the seasonal footprinting mechanism using coupled model experiments. *J Clim* 23:2885–2901

Allan R, Ansell T (2006) A new globally complete monthly historical gridded mean sea level pressure dataset (HadSLP2): 1850–2004. *J Clim* 19:5816–5842

Anderson BT (2003) Tropical Pacific sea-surface temperatures and preceding sea level pressure anomalies in the subtropical North Pacific. *J Geophys Res* 108:D23. doi:[10.1029/2003JD003805](https://doi.org/10.1029/2003JD003805)

Anderson BT (2004) Investigation of a large-scale mode of ocean–atmosphere variability and its relation to tropical Pacific sea surface temperature anomalies. *J Clim* 17:4089–4098

Anderson BT, Perez RC, Karspeck A (2013) Triggering of El Niño onset through trade wind-induced charging of the equatorial Pacific. *Geophys Res Lett* 40:1212–1216. doi:[10.1002/grl.50200](https://doi.org/10.1002/grl.50200)

Andreoli RV, Kayano MT (2005) ENSO-related rainfall anomalies in South America and associated circulation features during warm and cold Pacific decadal oscillation regimes. *Int J Climatol* 25:2017–2030

Arblaster JM, Meehl GA (2006) Contributions of external forcings to southern annular mode trends. *J Clim* 19:2896–2905

Arblaster JM, Meehl GA, Moore AM (2002) Interdecadal modulation of Australian rainfall. *Clim Dyn* 18:519–531

Bjerknes J (1969) Atmospheric teleconnections from the equatorial Pacific. *Mon Weather Rev* 97:163–172

Bretherton CS, Smith C, Wallace JM (1992) An intercomparison of methods for finding coupled patterns in climate data. *J Clim* 5:541–560

Chang P, Zhang L, Saravanan R, Vimont DJ, Chiang JCH, Ji L, Seidel H, Tippett MK (2007) Pacific meridional mode and El Niño–Southern Oscillation. *Geophys Res Lett* 34:L16608. doi:[10.1029/2007GL030302](https://doi.org/10.1029/2007GL030302)

Chiang J, Vimont DJ (2004) Analogous Pacific and Atlantic meridional modes of tropical atmosphere–ocean variability. *J Clim* 17:4143–4158

Compo GP, Sardeshmukh PD (2004) Storm track predictability on seasonal and decadal scales. *J Clim* 17:3701–3720

Compo GP et al (2011) The twentieth century reanalysis project. *Q J R Meteorol Soc* 137:1–28

Ding QH, Steig EJ, Battisti DS, Wallace JM (2012) Influence of the tropics on the Southern Annular Mode. *J Clim* 25:6330–6348

Ding RQ, Li JP, Tseng YH, Sun C, Guo YP (2015a) The Victoria mode in the North Pacific linking extratropical sea level pressure variations to ENSO. *J Geophys Res* 120:27–45. doi:[10.1002/2014JD022221](https://doi.org/10.1002/2014JD022221)

Ding RQ, Li JP, Tseng YH (2015b) The impact of South Pacific extratropical forcing on ENSO and comparisons with the North Pacific. *Clim Dyn* 44:2017–2034

Fogt RL, Bromwich DH (2006) Decadal variability of the ENSO teleconnection to the high-latitude South Pacific governed by coupling with the Southern Annular Mode. *J Clim* 19:979–997

Gershunov A, Barnett TP (1998) Interdecadal modulation of ENSO teleconnections. *Bull Am Meteorol Soc* 79:2715–2725

Giese BS, Ray S (2011) El Niño variability in simple ocean data assimilation (SODA), 1871–2008. *J Geophys Res* 116:C02024. doi:[10.1029/2010JC006695](https://doi.org/10.1029/2010JC006695)

Gillett NP, Thompson DWJ (2003) Simulation of recent Southern Hemisphere climate change. *Science* 302:273–275

Gong DY, Wang SW (1999) Definition of Antarctic oscillation index. *Geophys Res Lett* 26:459–462. doi:[10.1029/1999GL900003](https://doi.org/10.1029/1999GL900003)

Gutzler DS, Kann DM, Thornbrugh C (2002) Modulation of ENSO-based long-lead outlooks of Southwestern US winter precipitation by the Pacific decadal oscillation. *Weather Forecast* 17:1163–1172

Horel JD, Wallace JM (1981) Planetary-scale atmospheric phenomena associated with the Southern Oscillation. *Mon Weather Rev* 109:813–829

Hoskins BJ, Karoly DJ (1981) The steady linear response of a spherical atmosphere to thermal and orographic forcing. *J Atmos Sci* 38:1179–1196

Hu ZZ, Huang BH (2009) Interferential impact of ENSO and PDO on dry and wet conditions in the US great plains. *J Clim* 22:6047–6065

Hunt BG, Elliott TI (2003) Secular variability of ENSO events in a 1000-year climatic simulation. *Clim Dyn* 20:689–703

Ishii M, Shouji A, Sugimoto S, Matsumoto T (2005) Objective analyses of sea-surface temperature and marine meteorological variables for the 20th century using ICOADS and the Kobe collection. *Int J Climatol* 25:865–879

Jin D, Kirtman BP (2009) Why the Southern Hemisphere ENSO responses lead ENSO? *J Geophys Res* 114:D23101. doi:[10.1029/2009JD012657](https://doi.org/10.1029/2009JD012657)

Kalnay E et al (1996) The NCEP–NCAR 40-year reanalysis project. *Bull Amer Meteor Soc* 77:437–471

Kim JW, Yeh SW, Chang EC (2013) Combined effect of El Niño–Southern Oscillation and Pacific Decadal Oscillation on the East Asian winter monsoon. *Clim Dyn* 42:957–971

Kwok R, Comiso JC (2002) Southern Ocean climate and sea ice anomalies associated with the Southern Oscillation. *J Clim* 15:487–501

L'Heureux ML, Thompson DWJ (2006) Observed relationships between the El Niño–Southern Oscillation and the extratropical zonal-mean circulation. *J Clim* 19:276–287

Li Y, Li JP, Feng J (2012) A teleconnection between the reduction of rainfall in southwest Western Australia and north China. *J Clim* 25:8444–8461

Li XF, Yu JJ, Li Y (2013) Recent summer rainfall increase and surface cooling over Northern Australia: a response to warming in the tropical Western Pacific. *J Clim* 26:7221–7239

Madden RA, Julian PR (1994) Observations of the 40–50-day tropical oscillation—a review. *Mon Weather Rev* 122:814–837

Mann ME, Bradley RS, Hughes MK (2000) Long-term variability in the El Niño/Southern Oscillation and associated teleconnections. In: Diaz HF, Markgraf V (eds) El Niño and the Southern Oscillation: multiscale variability and global and regional impacts. Cambridge University Press, Cambridge, pp 357–412

Mantua NJ, Hare SR, Zhang Y, Wallace JM, Francis RC (1997) A Pacific interdecadal climate oscillation with impacts on salmon production. *Bull Am Meteorol Soc* 78:1069–1079

Marshall GJ, Stott PA, Turner J, Connolley WM, King JC, Lachlan-Cope TA (2004) Causes of exceptional atmospheric circulation changes in the Southern Hemisphere. *Geophys Res Lett* 31:L14205. doi:[10.1029/2004GL019952](https://doi.org/10.1029/2004GL019952)

McCabe GJ, Dettinger MD (1999) Decadal variations in the strength of ENSO teleconnections with precipitation in the western US. *Int J Climatol* 19:1399–1410

McPhaden MJ (1999) Genesis and evolution of the 1997–98 El Niño. *Science* 283:950–954

McPhaden MJ, Bahr F, Du Penhoat Y, Firing E, Hayes SP, Niiler PP, Richardson PL, Toole JM (1992) The response of the western equatorial Pacific Ocean to westerly wind bursts during November 1989 to January 1990. *J Geophys Res* 97:14289–14303

Mo KC (2000) Relationships between low-frequency variability in the Southern Hemisphere and sea surface temperature anomalies. *J Clim* 13:3599–3610

Mo KC, Ghil M (1987) Statistics and dynamics of persistent anomalies. *J Atmos Sci* 44:877–901

Pavia EG, Graef F, Reyes J (2006) PDO–ENSO effects in the climate of Mexico. *J Clim* 19:6433–6438

Power S, Casey T, Folland C, Colman A, Mehta V (1999) Interdecadal modulation of the impact of ENSO on Australia. *Clim Dyn* 15:319–324

Power SB, Haylock MH, Colman R, Wang X (2006) The predictability of inter-decadal changes in ENSO activity and ENSO teleconnections. *J Clim* 19:4755–4771

Pyper BJ, Peterman RM (1998) Comparison of methods to account for autocorrelation in correlation analyses of fish data. *Can J Fish Aquat Sci* 55:2127–2140

Rayner NA, Brohan P, Parker DE, Folland CK, Kennedy JJ, Vanicek M, Ansell T, Tett SFB (2006) Improved analyses of changes and uncertainties in sea surface temperature measured in situ since the mid-nineteenth century: the HadSST2 dataset. *J Clim* 19:446–469

Renwick JA (2002) Southern Hemisphere circulation and relationships with sea ice and sea surface temperature. *J Clim* 15:3058–3068

Renwick JA, Revell MJ (1999) Blocking over the South Pacific and Rossby wave propagation. *Mon Weather Rev* 127:2233–2247

Rogers JC (1981) The North Pacific Oscillation. *J Climatol* 1:39–57

Sardeshmukh PD, Hoskins BJ (1988) The generation of global rotational flow by steady idealized tropical divergence. *J Atmos Sci* 45:1228–1251

Seager R, Harnik N, Kushnir Y, Robinson W, Miller J (2003) Mechanisms of hemispherically symmetric climate variability. *J Clim* 16:2960–2978

Shimizu MH, Cavalcanti IFD (2011) Variability patterns of Rossby wave source. *Clim Dyn* 37:441–454

Smith TM, Reynolds RW, Peterson TC, Lawrimore J (2008) Improvements to NOAA's historical merged land–ocean surface temperature analysis (1880–2006). *J Clim* 21:2283–2296

Straus DM, Shukla J (2002) Does ENSO force the PNA? *J Clim* 15:2340–2358

Sun C, Li JP, Feng J, Xie F (2015) A decadal-scale teleconnection between the North Atlantic oscillation and subtropical eastern Australian rainfall. *J Clim* 28:1074–1092

Thompson DWJ, Solomon S (2002) Interpretation of recent Southern Hemisphere climate change. *Science* 296:895–899

Thompson DWJ, Wallace JM (2000) Annular modes in the extratropical circulation. Part I: month-to-month variability. *J Clim* 13:1000–1016

Trenberth KE, Shea DJ (1987) On the evolution of the Southern Oscillation. *Mon Weather Rev* 115:3078–3096

Vimont DJ, Battisti DS, Hirst AC (2001) Footprinting: a seasonal connection between the tropics and mid-latitudes. *Geophys Res Lett* 28:3923–3926

Vimont DJ, Wallace JM, Battisti DS (2003a) The seasonal footprinting mechanism in the Pacific: implications for ENSO. *J Clim* 16:2668–2675

Vimont DJ, Battisti DS, Hirst AC (2003b) The seasonal footprinting mechanism in the CSIRO general circulation models. *J Clim* 16:2653–2667

Walker GT, Bliss EW (1932) World weather. V *Mem R Meteorol Soc* 4:53–84

Wallace JM, Gutzler DS (1981) Teleconnections in the geopotential height field during the northern hemisphere winter. *Mon Weather Rev* 109:784–812

Wang XL, Ropelewski CF (1995) An assessment of ENSO-scale secular variability. *J Clim* 8:1584–1599

Wang B, Wang Y (1996) Temporal structure of the Southern Oscillation as revealed by waveform and wavelet analysis. *J Clim* 9:586–1598

Wang L, Chen W, Huang RH (2008) Interdecadal modulation of PDO on the impact of ENSO on the East Asian winter monsoon. *Geophys Res Lett* 35:L20702. doi:[10.1029/2008GL035287](https://doi.org/10.1029/2008GL035287)

Wu ZW, Li JP, Wang B, Liu XH (2009) Can the Southern Hemisphere annular mode affect China winter monsoon? *J Geophys Res* 114:D11107. doi:[10.1029/2008JD011501](https://doi.org/10.1029/2008JD011501)

Wu ZW, Li JP, Jiang ZH, Ma TT (2012) Modulation of the Tibetan Plateau snow cover on the ENSO teleconnections: from the East Asian summer monsoon perspective. *J Clim* 25:2481–2489

Wu ZW, Dou J, Lin H (2015) Potential influence of the November–December Southern Hemisphere annular mode on the East Asian winter precipitation: a new mechanism. *Clim Dyn* 44:1215–1226

Xie SP, Philander SGH (1994) A coupled ocean–atmosphere model of relevance to the ITCZ in the eastern Pacific. *Tellus* 46A:340–350

Yu JY, Kim ST (2011) Relationships between extratropical sea level pressure variations and the central Pacific and eastern Pacific types of ENSO. *J Clim* 24:708–720

Yu JY, Paek H, Saltzman E, Lee T (2015) The early-1990s change in ENSO–PSA–SAM relationships and its impacts on Southern Hemisphere climate. *J Clim*. doi:[10.1175/JCLI-D-15-0335.1](https://doi.org/10.1175/JCLI-D-15-0335.1)

Yuan XJ (2004) ENSO-related impacts on Antarctic sea ice: a synthesis of phenomenon and mechanisms. *Antarct Sci* 16:415–425

Zhang Y, Wallace JM, Battisti DS (1997) ENSO-like interdecadal variability. *J Clim* 10:1004–1020